Detection and Visibility Estimation of Surface Defects under Various Illumination Angles using Bidirectional Reflectance Distribution Function and Local Binary Pattern

Petra Gospodnetić
Department of Electronic Systems and Information Processing
University of Zagreb, Faculty of Electrical Engineering and Computing, Croatia
petra.gospodnetic@gmail.com

Falco Hirschenberger
Department of Image Processing
Fraunhofer-Institut für Techno- und Wirtschaftsmathematik
Kaiserslautern, Germany
falco.hirschenberger@itwm.fraunhofer.de

***Abstract* – In the development of surface defect inspection systems, the surface illumination often plays a key role for the detectability of the defect. The illumination setup is currently configured manually for each type of defect which needs to be detected. This paper presents the use of a local binary pattern operator together with the bidirectional reflectance distribution function in order to detect various surface defects and estimate their visibility. This method is useful for improving the reliability of the visual surface inspection system and shortening of the time required for conducting a feasibility study. The reflectance of the sample material is acquired through a custom-built image acquisition system, which uses a robot arm in order to automatically retrieve the data under different illumination angles. By combining texture description with reflectance information, it is possible to localize defects without prior knowledge of their characteristics, whereas the defect visibility estimation requires manual ground truth marking in order to produce realistic results.**

Keywords – local binary pattern, image acquisition, surface defect detection, bidirectional reflectance, distribution function, visibility estimation, illumination set-up, texture analysis

I. INTRODUCTION

Automatic visual surface inspection through image processing is a method of non-invasive surface quality inspection for industrial purposes. Even though the implementation of the inspection system appears quite straightforward at first, the detection process soon becomes complex since there is no unambiguous parameterized definition of a defect and its image varies with surface properties such as material, texture and reflectivity. Attempts [1] have been made to define the surface defects descriptively by their shape and source of origin. Since such approaches are inefficient and unreliable, various texture analysis approaches have been proposed [2], but all of them are relying on a stable defect visibility. Therefore, the first step in the development of an inspection system is to make the visibility of each defect stable by determining the appropriate light conditions during the image acquisition phase. The adjustment of the light conditions is done manually, the visibility of a defect is determined heuristically and the duration of the overall process is often measured in days.

In this paper we propose a method for an automatic defect detection, additionally expanded with a defect visibility evaluation. The main advantage of the proposed defect detection method is that it requires no previous knowledge of the defect characteristics. It is carried out using a combination of the bidirectional reflectance distribution function (BRDF) and local binary patterns (LBP). The BRDF-LBP approach combines surface light response (radiance) information with its illumination-dependent texture characteristics in order to distinguish the defective from the correct surface. The visibility of the detected defects is further evaluated using manual ground truth marking in order to obtain the ratio of the found defect size to the ground truth size.

BRDF data is traditionally measured using gonioreflectometers [3], but Ward [4] introduced one of the first methods which used a digital camera instead. In [5] Dana extended the measurement and use of the BRDF for investigation of the visual appearance of real-world surfaces and the dependence of their appearance on imaging conditions. In order to obtain persistent image acquisition conditions, a robot arm was introduced into the setup as a sample holder. In their work, camera angles were changed manually and the light source was fixed, whereas in our paper a somewhat different setup was used – both the camera and the sample plane were fixed, while the robot arm carried the light source.

Defect detection using the LBP operator has already been proven useful for surface defect identification and localization for patterned fabric [6]. It has often been used for texture classification ([2], [7], [8]), while in [9] it was used in combination with a self-organizing map as a classifier for real-time paper surface inspection. For the purpose of this paper, LBP is used as a method for confirmation of the discovered BRDF defect candidates.

As far as known from the available literature [2], surface defect detection has been done using different approaches (statistical, structural, filterbased, modelbased) in order to identify potential defect candidates, but a visibility factor has

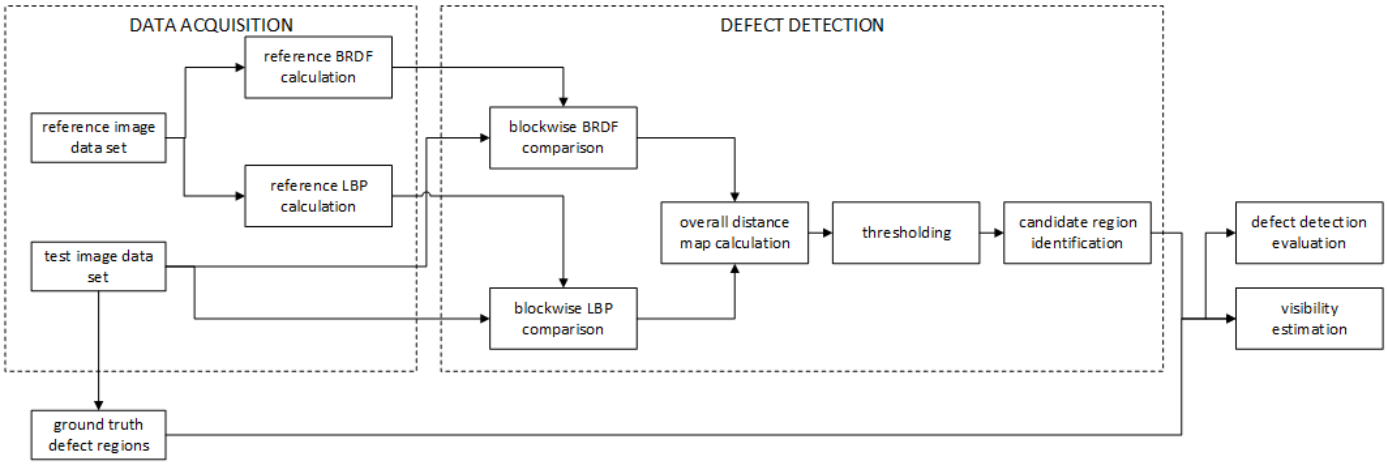

Figure 1 BRDF-LBP method pipeline

been presented only once before by Muehlemann [1], who used no defect detection but instead used manual extraction of a pixel vector across the center for each found defect in order to evaluate the amount of contrast change within the area. On the contrary, this paper proposes an approach which requires only one ground truth image to be used in the visibility estimation.

Further, in chapter II of this paper the methods contributing to our approach will be introduced, followed by the presentation of the obtained results in chapter III and the conclusion in chapter IV.

II. Materials and Methods

The surface texture in an image is a planar representation of the surface geometry, shaped by the highlights and the shadows of the present microstructure. Therefore its texture characteristics will change with the light conditions under which the image is acquired. A defect can be defined as an unwanted change in surface geometry and/or color. For a flat homogeneous material, the texture is uniformly spread and the surface radiance is consistent, which implies that any defect would be represented as a change in texture pattern and radiance. The method used to find and evaluate defects in such a way has three main steps, as presented in Figure 1:

- data acquisition through a parameterized image acquisition and the BRDF and LBP feature extraction;
- defect detection through a comparison of the test sample features to the reference sample features; and
- evaluation of the defect detection process and defect visibility estimation through the comparison of obtained defect candidates to manually marked ground truth defects.

A. Image acquisition

Obtaining measurable and reproducible image acquisition conditions required the construction of a standalone custom acquisition setup represented in Figure 2. It consisted of three main parts: a fixed camera, a movable light source and a flat sample plate. Since the main goal of this work was to assess the defect visibility for various light angles, all other system variables needed to be fixed. Therefore the camera was always mounted perpendicular to the sample surface with a fixed resolution, focal length and aperture. The light source was mounted on a robotic arm, which allowed for the light source to be moved incrementally by an angle of θ over the plate, following a precise arch line. In that way only the light angle α towards the camera was being changed, while maintaining other light source characteristics such as incident irradiance, distance and orientation fixed in relation to the surface plane.

For each new $\theta \epsilon [0, \pi]$, a new image was acquired. Variation of the angle α implied a variation in surface radiance, where the difference between the minimum and the maximum radiance was likely to exceed the dynamic range of the camera, thus providing images with marginal conditions (under- and overexposed images), as visible in Figure 3. While images with marginal conditions contain less information, it is possible that some defects may be easier to distinguish in that way. Therefore, these images should not be excluded from the further analysis. The complete data acquisition required that each light position be captured with an appropriate exposure. In order to fulfill this requirement, as well as to obtain the marginal conditions, multiple acquisition arches were repeated, with each arch having a constant exposure time.

The exact exposure time of each acquisition arch was determined using an automatic exposure evaluation, as presented in [10]. The exposure time used for the first acquisition arch was evaluated for the first image to be acquired. All images acquired in one acquisition arch were further marked as being either correct or incorrect by measuring the mean value of each image. If the mean value was not in the central interval of the pixel value range, the image was considered to be incorrectly exposed.

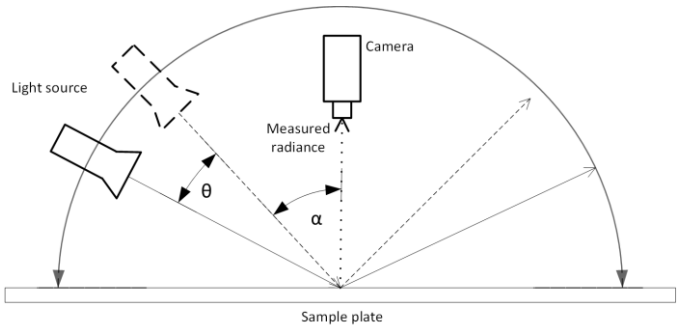

Figure 2 Image acquisition setup

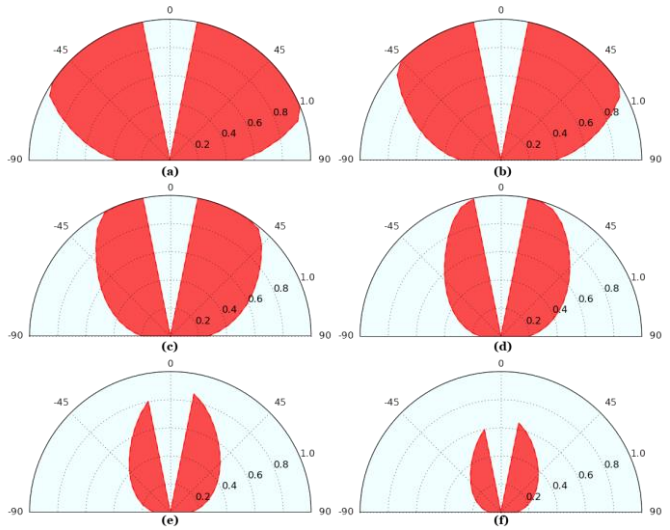

Figure 3 BRDF response for six acquisition arches, where the red field represents the acquired reflectance response of the sample at angles of -80 to 80 degrees, with an increment θ of five degrees. The exposure time used for the acquisition shortens from (a) to (f) respectively.

Further exposure evaluation was done by evaluating the first light position for which the image was marked as incorrect in the preceding acquisition. The process was repeated until each light position was captured with an appropriate exposure in at least one of the acquisition arches.

Exposure times were evaluated only for the reference sample acquisition and were afterwards saved. The saved exposure times were later used in the test sample acquisition in order to ensure that the test sample was acquired under the same conditions as the reference sample.

B. *Feature extraction*

When light hits a surface, it is either reflected, transmitted or absorbed. For opaque materials, the majority of the incident light is transformed into reflected and absorbed light. BRDF f_r [11] provides a complete reflectance information of an opaque surface at a single point x and is evaluated as the ratio of the radiance L exiting the surface in a given direction to the incident irradiance I from an incident solid angle $d\omega_i$ at a given illumination direction, as represented in Figure 4.

$$f_r(\theta_i, \varphi_i, \theta_e, \varphi_e) = \frac{dL(\theta_e, \varphi_e)}{dI(\theta_i, \varphi_i)} \tag{1}$$

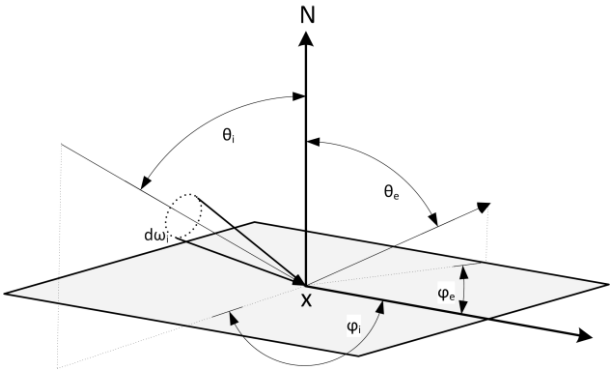

Figure 4 Surface reflection model

For the purpose of this work, the surface of a sample plate was assumed to be an isotropic material as proposed in [12], thus making the reflectance independent of the rotation of the incident and emerging directions about the surface normal, and dependent only on their relative difference $\Delta\varphi = \varphi_e - \varphi_i$. Therefore the BRDF function used for this work is dependent only on three variables $f_r(\theta_i, \theta_e, \Delta\varphi)$, of which θ_e and $\Delta\varphi$ were fixed throughout the acquisition process.

The LBP operator, originally introduced by [13], is a computationally efficient and monotonic gray-scale change invariant operator, commonly used for texture classification. The motivation for using LBP in defect visibility estimation came from the assumption that the defects were represented as a change of pattern within the surface texture and were therefore detectable when compared to a previously acquired reference pattern. The LBP operator labels the image pixels by comparing each of them to its 3x3 neighborhood and summing the results as weighted values by the power of two (2) if the neighborhood pixel is greater than or equal to the center pixel. Since textures can come in different sizes and rotations, the LBP operator was later extended in two ways [13]: to use neighborhoods of various sizes and to use only uniform binary patterns as descriptors. Neighborhoods of different sizes were determined by (P, R), where P represented the number of sampling points and R was the radius of the neighborhood. In that case the sampling points were evenly spaced on a circle around the central pixel g_c with coordinates (x, y) and a sample point pixel g_p whose coordinates were given by $(x_p, y_p) = (x + R\cos(2\pi p/P), y - R\sin(2\pi p/P))$, where $p \in [0, P-1]$. The function s was used to exclude the difference between g_c and g_p from the overall sum if g_p was greater than g_c. When sampling point coordinates did not fall in the center of a pixel, bilinear interpolation was used for an estimation of the value in that point. Uniform patterns were introduced in order to make operator rotation invariant. A pattern is considered uniform only if the pattern contains no more than two bitwise transitions from 0 to 1 or vice versa. In the computation of the LBP histograms, uniform patterns were assigned separate bins, while non-uniform patterns are assigned to a single bin. That way, for a 3x3 neighborhood, there were only 58, instead of 256 different patterns.

$$LBP_{P,R} = \sum_{p=0}^{P-1} s(g_p - g_c)2^p,$$
$$s(x) = \begin{cases} 1, & if\ x \geq 0 \\ 0, & otherwise \end{cases} \tag{2}$$

C. *Defect detection*

For each acquired image in the reference image data set both BRDF and LBP were calculated separately (Figure 1) for later use as baseline features. As both the reference and the test sample were acquired under the same conditions, the defect detection process was always comparing two images (one from the reference set and one from the test set) corresponding in light position and exposure time. By comparing the corresponding images, we searched for deviations from the baseline features.

Baseline BRDF features described a mean expected reflectance response of the material at a given position and were compared to the mean reflectance response in 5x5 sub-blocks of the test sample image. At the same time, the baseline LBP

features described the reference sample image divided into 40x40 sub-blocks, meaning that every block was described with its own LBP histogram.

The BRDF and LBP comparison results were given as two 2D distance maps, both matching pixel positions of the original test sample image. The BRDF map represented a distance from the expected reflectance response, while the LBP map was obtained by dividing the test image in the same manner as the reference image, into 40x40 sub-blocks, and then comparing the LBP histograms of the corresponding sub-block. Histograms were compared using χ^2 metrics (3), where h_1 and h_2 denote the reference sample histogram and test sample histogram respectively.

$$\chi^2(h_1, h_2) = \sum_{i=0}^{n-1} \frac{(h_{1_i} - h_{2_i})^2}{h_{1_i} + h_{2_i}} \quad (3)$$

Fusing the BRDF with the LBP feature calculation allowed us to apply the discriminative power of the LBP operator with the sensitivity of the BRDF to radiance changes. As visible from Figure 5, the distance maps obtained from the comparison of the reference and the test images were fused by multiplication. This multiplication resulted in mutual noise cancellation and an overall increase in solid defect labeling with more precision regarding its shape. Binarization of the newly acquired distance map was performed by low-level thresholding in order to remove the possible low-intensity noise, after which a

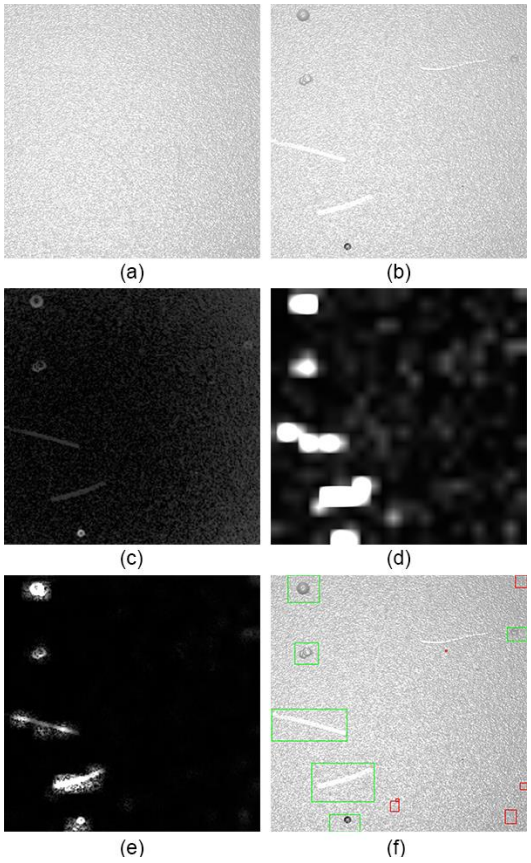

Figure 5 (a) - (f) Candidate region identification procedure for an image of a plastic board (sample 1): (a) reference sample image; (b) test sample image; (c) BRDF distance map; (d) LBP distance map; (e) BRDF-LBP distance map fusion; (f) detected defect candidates.

morphological dilation and closing was applied in order to connect candidates which may belong to the same defect. Values of both the low-level thresholding and the morphological operations were constant throughout the defect detection process. For the purpose of this work, they were determined heuristically.

D. Defect detection process and visibility estimation

At the beginning of the process, a user is given one well exposed image of the test sample and asked to mark known defects in the image, regardless of whether he may think them to be detectable or not in the further process. This image is then used twofold as ground truth: in the evaluation of the defect detection process and for visibility estimation. After the defect detection step, the identified candidate regions were being compared to the ground truth defect regions P. If they overlaped, the candidate was considered a true positive TP, whereas otherwise it was a false positive FP. From the obtained data, the defect detection process was evaluated by two measures: by the precision, also known as positive predictive value (PPV), and by the sensitivity, known as true positive rate (TPR):

$$PPV = \frac{TP}{TP + FP} \quad (4)$$

$$TPR = \frac{TP}{P} \ . \quad (5)$$

For the purpose of this paper we defined the defect visibility $v(D)$ as a relative size of the candidate region $R(C)$ to the ground truth defect region $R(D)$. A reason for this lies in the assumption that a bigger candidate implies a bigger spatial and textural deviation. It is a frequent occurrence that one defect is represented by more than one candidate, in which case the regions of all the candidates corresponding to the evaluated defect are summed up first and then compared to the ground truth region.

$$v(D) = \frac{\sum R(C_D)}{R(D)} \quad (6)$$

E. Experimental details

In order to perform the defect detection and visibility estimation, two samples of the same material were needed: the reference sample representing a defect-free surface and the test sample representing a surface containing various texture defects. For the purpose of this paper, the used reference sample surfaces were flat semi-glossy homogeneous materials: a white plastic board (sample 1) and a black metal-elastomer plate (sample 2).

The image acquisition was carried out using a UR10CB2 robot arm carrying a LED light source EFFI-Flex_5_525_1_3 of the wavelength 525 nm, with a diffused window and the lens set to the highest position. The distance between the light source and the sample plate was set to 0.53 m, at which point the illuminance was close to 1500 Lux, according to the official datasheet [14]. The camera used was a Basler industrial camera acA2500-14gm of resolution 2592 px ×1944 px, mounted with a Kowa 16mm/F 1.4 lens at the distance of 0.28 m. The acquisition process was fully automatic. The acquisition arches were repeated until all the light positions were imaged with an appropriate exposure as explained in section II.A. The duration of one acquisition arch was approximately 90 seconds.

III. RESULTS

The proposed BRDF-LBP approach was evaluated on two different homogeneous materials, as described in II.E, both containing various undefined textural defects. By *undefined*, we assume that the defect detection process had no prior knowledge of the defect locations or even of their existence. The ground truth marked image was used only for the evaluation of the process results and calculation of the defect visibility.

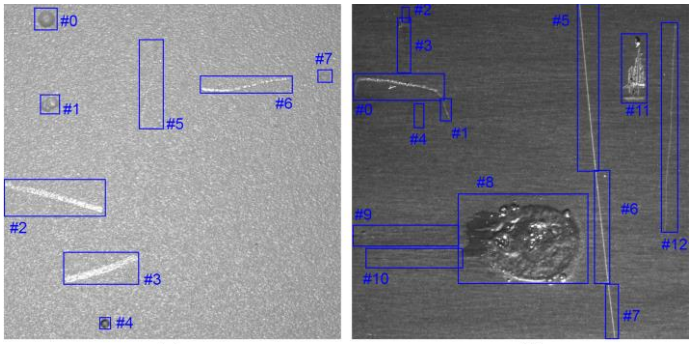

Figure 6 Numbered ground truth defect regions: (a) white plastic board (sample 1) and (b) black metal-elastomer plate (sample 2).

The white board sample contained eight different defects, while the metal-elastomer one contained ten. As can be seen from the ground truth image in Figure 6, some defects were split into sub-defects due to their size and orientation. Here we will present the defect detection performance (Table 1) and visibility plots for several specific defects from both samples. The selection of the presented results is based on the avoidance of redundancies resulting from the similarity of the defects. Defects of similar size and texture pattern produce similar visibility results.

Table 1 shows that the defect detection process had a high overall precision, while the overall sensitivity stayed around 55%. The sensitivity of the defect detection was expected and confirmed the assumption that an illumination angle revealed certain defects, while at the time hiding others. The results presented in Table 1 can be used as a baseline for future work on defect visibility calculation enhancement and automatization.

TABLE 1 DEFECT DETECTION PROCESS EVALUATION FOR WHITE PLASTIC BOARD (SAMPLE 1) AND BLACK METAL-ELASTOMER PLATE (SAMPLE 2)

	Sample 1		Sample 2	
Acquisition arch	**Precision [%]**	**Sensitivity [%]**	**Precision [%]**	**Sensitivity [%]**
1	80.5	55.7	55.9	57.4
2	85.7	56.2	71.5	70.7
3	86.6	59	88.7	62.5
4	89.5	62.	94.9	33.3
5	93.4	59.5		
6	96.7	52.9		
7	97.2	50		

A comparison of the identified candidates and ground truth defect positions by size and position resulted in visibility plots shown in Figure 7 (sample 1) and Figure 8 (sample 2). The visibility was plotted over 180 degrees for all obtained acquisition arches, for each defect separately. A visibility value of 1 marks high visibility whereas 0 marks no visibility. As can be noticed, all plots have a data gap between 85 and 95 degrees. The reason for this gap is of a technical nature – the camera was set directly above the sample plate and hence was casting a shadow, making the data acquisition impossible for those illumination angles.

The defect in Figure 7 (a) was a very sharp bump which was mostly visible since it clearly changed texture for the various illumination angles, whereas defect 2 in Figure 7 (b) had a very high peak for acquisition 6 (shortest exposure time), and was otherwise not clearly distinguishable. In Figure 7 (c) we can notice the shift of the visibility towards the perpendicular illumination angle as the exposure time shortened. Figure 7 (d) demonstrates that defect #5 would be visible from angles of around 70 degrees and 125 degrees.

Figure 8 shows that the defects on the metal-elastomer plate have their visibility peaks spread over the arch. Such results may be explained by metal-derived phenomena. Since the metal-elastomer plate is of a compound material of rubber and metal, it may partially exhibit specular reflections, which is a characteristic of metal. The specular component should not be treated as a problem for the purpose of this paper, but a further study should be made on the defect behavior on non-isotropic surfaces.

The overall process, including the execution of both the defect detection and the visibility estimation lasted approximately 30 minutes for sample 1 and approximately 20 minutes for the sample 2. The process included automatic image acquisition and defect detection, manual ground truth marking and visibility estimation.

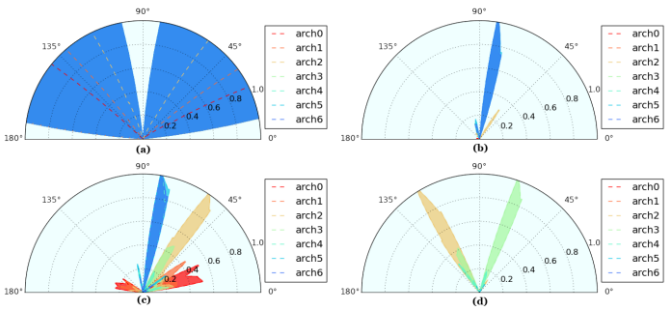

Figure 7 Visibility plots for four specific defects found on white board (sample 1): (a) defect #0; (b) defect #2; (c),defect #3; (d) defect #5

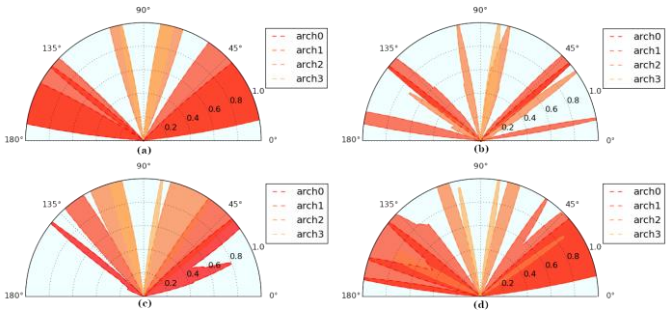

Figure 8 Visibility plots for four specific defects found on black metal-elastomer plate (sample 2): (a) defect #1; (b) defect #5; (c) defect #9; (d) defect #12

IV. Conclusion

The defect detection method using a combination of LBP and BRDF confirmed the possibility of surface defect detection without prior knowledge of the defect characteristics. The results presented in this paper show that the method yields high defect detection precision rates for materials having uniformly textured and nearly isotropic surfaces.

The introduced method shows stable and promising results for two samples. The samples were made of different materials, confirming that the method can be material-independent. This has to be evaluated further in order to achieve a verification of the method.

The expansion of the defect detection process with the defect visibility estimation makes our method very suitable for improving the design and development of visual surface inspection systems. The automatization of the image acquisition process ensures a precision which can hardly be obtained manually, as well as reproducibility. As previously stated, the process of manual visibility estimation is often measured in days. Therefore the time obtained in the presented work shows a significant improvement towards shortening the duration of the feasibility study.

References

[1] M. Muehlemann, "Standardizing Defect Detection for the Surface Inspection of Large Web Steel," 2000. [Online]. Available: http://www.illuminationtech.com/documents/surface_inspection.pdf. [Accessed 18 10 2015].

[2] X. Xie, "A Review of Recent Advances in Surface Defect Detection using Texture Analysis Techniques," *Electronic Letters on Computer Vision and Image Analysis*, vol. 7, no. 3, pp. 1-22, 2008, doi: 10.5565/rev/elcvia.268

[3] S. C. Foo, "A gonioreflectometer for measuring bidirectional reflectance of material for use in illumination computation.," Master's thesis, Cornell University, 1997.

[4] G. J. Ward, "Measuring and Modeling Anisotropic Reflection," *Computer Graphics*, no. 26, pp. 265-273, 1992.

[5] K. J. Dana, B. van Ginneken, S. K. Nayar and J. J. Koenderink, "Reflectance and Texture of Real-World Surface," *ACM Transactions on Graphics*, vol. 18, no. 1, pp. 1-34, 1999.

[6] F. Tajeripour, E. Kabir and A. Sheikhi, "Defect Detection in Patterened Fabrics using Modified Local Binary Patterns," in *International Conferrence on Computational Intelligence and Multimedia Applications*, 2007, doi: 10.1155/2008/783898

[7] H. Y. T. Ngan, G. Kwok Hung Pan and N. Hon Ching Yung, "Automated fabric defect detection - a review," *Image and Vision Computing*, vol. 29, no. 7, pp. 42-458, 2011, doi: 10.1016/j.imavis.2011.02.002

[8] O. Ghita, P. F. Whelan, T. Carew and P. Nammalwar, "Quality Grading of Painted Slates Using Texture Analysis," *Computers in Industry*, vol. 56, pp. 802-815, 2005, doi: 10.1016/j.compind.2005.05.008

[9] T. Mäenpää, M. Turtinen and M. Pietikäinen, "Real-Time Surface Inspection by Texture," *Real-Time Imaging*, vol. 9, no. 5, pp. 289-296, 2003, doi: 10.1016/S1077-2014(03)00041-X

[10] S. Battiatio, G. Messina and A. Castorina, "Exposure Correction for Imaging Devices: an Overview," *ingle-Sensor Imaging, Methods and Applications for Digital Cameras, Image Processing Series*, 2008, doi: 10.1201/9781420054538.ch12

[11] S. R. Marschner, S. H. Westing, E. P. F. Lafortune, K. E. Torrance and D. P. Greenberg, "Image-Based BRDF Measurement Including Human Skin," *Rendering Techniques '99*, pp. 139-152, 1999.

[12] W. Matusik, H. Pfister, M. Brand and L. McMillan, "Efficient Isotropic BRDF Measurement," in *Eurographics Symposium on Rendering*, 2003.

[13] T. Ojala, "Multiresolution Gray-Scale and Rotation Invariant Texture Classificiation with Local Binary Patterns," *IEEE Transactions on Pattern Analysis and Machine Intelligence*, pp. 971-987, 2002, doi: 10.1109/TPAMI.2002.1017623

[14] effiLux, *Datasheet EFFI-Flex v.2.1*, Les Ulis, 2015.